Correlated Thermal Diffuse Scattering in Low to Medium Energy Electron Diffraction: A New Structural Tool

doi: 10.1103/PhysRevLett.82.335

Correlated Thermal Diffuse Scattering in Low to Medium Energy Electron Diffraction: A New Structural Tool

T. Abukawa,[1] C. M. Wei,[2] T. Hanano,[1] and S. Kono[1]
[1]*Research Institute for Scientific Measurements, Tohoku University, Sendai 980-8577, Japan*
[2]*Institute of Physics, Academia Sinica, Nankang, Taipei, Taiwan 11529, Republic of China*
(Received 27 August 1998)

We have observed simple oscillations in three-dimensional (3D) patterns of electron thermal diffuse scattering (separated from electron-electron energy loss) measured on a Si(001) surface. We interpret these oscillations as coherent interference within a small cluster of atoms in which vibrational correlation within the nearest neighbors (NN) is dominant. A 3D Patterson function analysis of the oscillation reveals the atomic structure of the Si(001) surface consisting of NN pairs including dimers. This finding provides a promising new clue to determine the structures of bulk and the surface of solids. [S0031-9007(98)08194-0]

PACS numbers: 61.14.Hg, 63.20.Kr, 68.35.Bs

The direct imaging of atomic structure is one of the most attractive subjects in surface science. Holographic reconstruction of atomic structures using photoelectron diffraction [1–3], Kikuchi electron diffraction (KED) [4,5], diffuse low energy electron diffraction (DLEED) [6,7], and very recent LEED holography [8] have been tested. These electron emission holographies (EEH) utilize the intensity oscillations that are generated by interference between the electron wave emitted from an atom and its single scattered waves by surrounding atoms [1–8]. However, single-energy EEH made limited success because of the large anisotropy of the atomic scattering factor $f(\theta)$ and the strong multiple scattering (MS) in electron diffraction. To overcome these problems, multienergy techniques were introduced [2–4,8]. KED, DLEED, and LEED holography are suitable for the multienergy holography because of the ease of changing the electron energy. However, DLEED is not applicable to the ordered surface structure [6,7]. LEED holography can be applied to ordered surfaces, but requires one prominent atom in the surface unit cell as a beam splitter. KED has provided a handy and powerful holographic technique that is applicable to ordered solid surfaces.

To further enrich the KED holography, we propose a new direct imaging technique by utilizing the correlated thermal diffuse scattering (CTDS) in low to medium energy (600–1500 eV) electron diffraction. In the CTDS, 2D intensity distribution of electrons that suffered only from phonon losses is measured in multienergy incidence. This is different from the KED holography where electrons that have undergone energy losses to electron systems are counted. Combined with the grazing incidence of an electron beam, CTDS may wear very high surface sensitivity. As it becomes clear later, CTDS is principally different from DLEED and LEED holography although the measurement of CTDS bears some similarities to that of DLEED. CTDS is based on the interference of scattered electron waves that have undergone phonon losses (defined as quasielastic scattering hereafter), while DLEED and LEED holography are based on the interference between the reference wave as elastically scattered (i.e., without phonon losses) by a beam-splitter atom and objective waves elastically scattered by the surrounding atoms. The measurements of CTDS, DLEED, and LEED holography include both elastically and quasielastically scattered electron waves because of the limited experimental energy resolutions. The electron energies in CTDS are substantially larger than those in DLEED and LEED holography, however.

The fundamental of the correlation effect on TDS is established in x-ray crystallography [9]. Since the vibrational correlation reduces the mean square relative displacements (MSRD) among near-neighbor atoms, an excess coherency, which causes structures in TDS, is generated. This can be explained by the phonon picture as the diffraction of short coherent-length electron waves created by phonon scattering. Thus, the structures are approximated by a Bragg reflection from a very small cluster of atoms [9]. On the analogy to the Patterson function analysis of Bragg spots, one may obtain the Patterson function of correlating atoms in crystal by an inverse Fourier transformation of the CTDS pattern. In this Letter, we report that the inverse Fourier transform of CTDS patterns of low to medium energy electron diffraction from a single-domain Si(001)-(2×1) surface indeed shows Patterson functions that involve clusters of nearest-neighbor (NN) Si atoms of bulk and surface.

Schematics of CTDS measurements are shown in Fig. 1a. A μ-electron beam of 600–1500 eV was incident at a grazing angle whose direction is represented by $\hat{\mathbf{k}}_i$. 2D intensity distribution of elastically and quasielastically scattered electrons was measured in a cone of 72°. A direction of a scattered electron within the cone is represented by $\hat{\mathbf{k}}$. The apparatus used has been described in detail elsewhere [10]. Briefly, it consisted of a μ-beam electron gun combined with a secondary electron detector, a micro-channel-plate (MCP) assisted RHEED screen, and a retarding field display (RFD) electron analyzer in

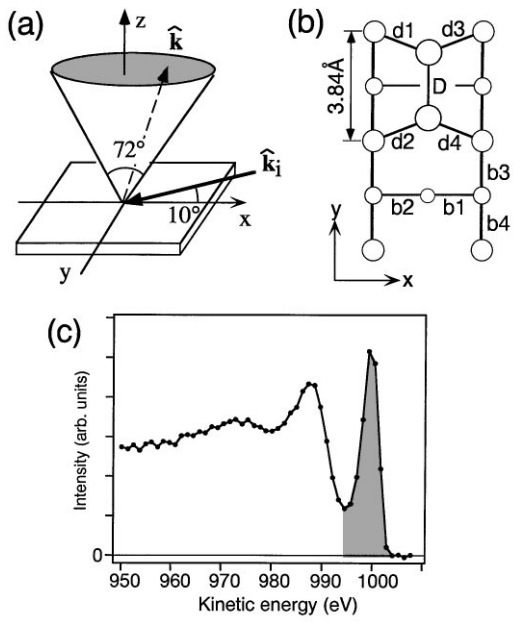

FIG. 1. (a) Schematics of CTDS measurements. (b) Symmetric dimer model of the Si(001)-(2 × 1) surface with the nearest-neighbor pairs labeled. (c) A typical energy distribution curve of electrons scattered from the Si(001)-(2 × 1) surface as measured by the RFD analyzer at a primary energy of 1000 eV.

a UHV chamber. The μ-beam electron gun can be used for scanning electron microscopy, RHEED, and CTDS. The RFD analyzer consisted of three concentric spherical grids and an assembly of a two-stage MCP and a phosphor screen. A fine mesh (350 lines/inch) was used for the central (retarding) grid of the RFD analyzer in order to achieve a good energy resolution. The displayed pattern was digitized with a CCD camera into a 150 × 150 matrix. A single-domain Si(001)-(2 × 1) surface, of which the domain ratio was confirmed to be 4:1 by RHEED, was prepared as reported previously [10]. The sample was so placed that the dimer bond of the major 2 × 1 domain points to the y axis as illustrated in Figs. 1a and 1b. Figure 1c is a typical energy distribution curve obtained by the RFD analyzer with a primary beam energy of 1000 eV. A peak at around 1000 eV is the elastic and quasielastic electrons and a peak at 987 eV is the plasmon-loss peak. For the CTDS measurements, the intensity of elastic and quasielastic electrons (under the shaded area) was counted. (The quasielastic electrons are dominant in the present energy and scattering-angle ranges.)

CTDS patterns at 21 wave numbers (from $k = 6.6$ (593 eV) to 10.6 a.u. (1529 eV) with an interval of 0.2 a.u.) were recorded. This made a 3D data set $I_{\hat{\mathbf{k}}_i}(k, \hat{\mathbf{k}})$ with angular points of ≈17 000 and radial points of 21. $I_{\hat{\mathbf{k}}_i}(k, \hat{\mathbf{k}})$ was normalized so as to make an integrated intensity within each radial point constant. Using the procedure described in Ref. [4], a background $B_{\hat{\mathbf{k}}}(k, \hat{\mathbf{k}})$ was created from the least-square fits of second-order polynomials to $I_{\hat{\mathbf{k}}}(k, \hat{\mathbf{k}})$ along the radial direction at each angular point. Then an oscillation χ is obtained as

$$\chi_{\hat{\mathbf{k}}_i}(k, \hat{\mathbf{k}}) = \frac{I_{\hat{\mathbf{k}}_i}(k, \hat{\mathbf{k}})}{B_{\hat{\mathbf{k}}_i}(k, \hat{\mathbf{k}})} - 1 . \quad (1)$$

This procedure eliminates the effect of direction dependent sensitivity of the RFD analyzer and cancels the intensity gradient caused by the atomic scattering factor.

An example of χ is shown in Figs. 2a and 2b; (a) is a cross section at $k = 7.2$ a.u. (706 eV) over the cone angle of 72° and (b) is a cross section at $\hat{k}_y = 0$ over the full energy range measured. Note that $\hat{\mathbf{k}}$ represents an angle. The incident beam was at 10° from the surface along the x axis from the right side as described already for Fig. 1.

It is surprising to see simple broad stripe experimental patterns in Figs. 2a and 2b. The sharp spots appearing on the left of Fig. 2a are due to surface Bragg spots (normal LEED spots), which can be eliminated by a filtering procedure [4]. The amplitude of oscillation of stripes is about 10% at lower k and is about 4% at higher k. These stripes form a multilayer structure in k space. To confirm the difference between CTDS and KED, we have measured KED patterns of the same energy range by setting the retarding grid voltage at 50 eV below the primary electron. The resulting χ function of KED patterns showed little oscillation along the k direction while the intensity varies along the emission angles. Thus, the stripes are specific to CTDS.

The simple stripes are due to the interference of electron waves scattered by a small number of NN atoms connected by vibrational correlation. In order to illustrate this we first show that the stripes are basically reproduced by the interference of electron waves from a single NN pair. The kinematical representation of electron intensity of waves scattered by two identical atoms at $\mathbf{r}_1$ and $\mathbf{r}_2$ is

$$I_{\hat{\mathbf{k}}_i}(k, \hat{\mathbf{k}}) \propto |f(k, \theta)e^{i\mathbf{s}\cdot\mathbf{r}_1} + f(k, \theta)e^{i\mathbf{s}\cdot\mathbf{r}_2}|^2 = 2|f(k, \theta)|^2(1 + \Re e^{i\mathbf{s}\cdot\mathbf{R}}) , \quad (2)$$

where $f(k, \theta)$, θ, $\mathbf{s} \equiv k(\hat{\mathbf{k}} - \hat{\mathbf{k}}_i)$, and $\mathbf{R} \equiv \mathbf{r}_2 - \mathbf{r}_1$ are the atomic scattering factor, the scattering angle, the scattering vector, and the relative position vector, respectively. With Eq. (2), we can calculate $I(\mathbf{k})$, thus $\chi(\mathbf{k})$, for a NN pair of Si(001). As labeled in Fig. 1b, there are four different kinds of bulk NN pairs, b1, b2, b3, and b4 and four NN dimer back-bond pairs, d1, d2, d3, and d4, and a dimer bond pair D. The symmetric dimer model is used since the buckling of dimers has not been resolved in this study although it may be possible in a more dedicated study. We find that the bulk NN pair b1 reproduces the experimental stripes rather well. The simulated $\chi(\mathbf{k})$ for the b1 pair is shown in Figs. 2c and 2d for the same conditions as in Figs. 2a and 2b, respectively. Although the curvature of stripes is different between Figs. 2a and 2c, the overall agreement is amazing. As shown later, the dimer back-bond NN pairs contribute to the difference. Thus, it is clear that the observed CTDS pattern is due to a cluster of atoms including the b1 NN pair.

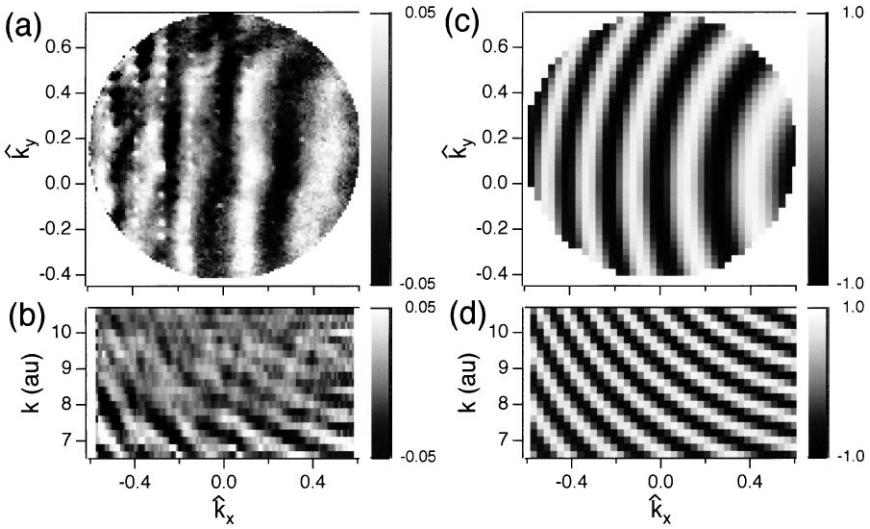

FIG. 2. (a) Cross section of the experimental χ function at $k = 7.2$ a.u. (b) Same as (a) but at $\hat{k}_y = 0$. (c) and (d) are the cross sections of χ function simulated for the nearest-neighbor pair of b1 in Fig. 1b, corresponding to (a) and (b), respectively.

If the observed CTDS pattern is due to a small cluster of correlated atoms, we can anticipate that an inverse Fourier transform of χ,

$$P(\mathbf{R}) = \left| \int \chi_{\hat{\mathbf{k}}_i}(\mathbf{s}) e^{-i\mathbf{s}\cdot\mathbf{R}} d\mathbf{s} \right|, \qquad (3)$$

gives the Patterson function or a self-correlation function [2,11]. Notice that Eq. (3) is different from the holographic reconstruction used in EEH where the exponential in Eq. (3) is $e^{-ik(\hat{\mathbf{k}}-\hat{\mathbf{r}})\cdot\mathbf{r}}$ [2,4]. $P(\mathbf{R})$ has a peak at $\mathbf{R} = \mathbf{r}_l - \mathbf{r}_m$, where $\mathbf{r}_l$ and $\mathbf{r}_m$ are atomic positions in crystal and has inversion symmetry, i.e., $P(\mathbf{R}) = P(-\mathbf{R})$. Since χ is used in Eq. (3) instead of intensity, $P(\mathbf{R})$ does not have a peak at the origin as the usual Patterson function has.

Figure 3 shows the calculated $P(\mathbf{R})$ from the experimental χ function of Fig. 2 using Eq. (3); (a) is a projection onto the xy plane, in which values up to $z = \pm 3$ Å are integrated, (b) and (c) are vertical cross sections at $y = 0$ and $x = a_0/2$ (= 1.92 Å), respectively. The images labeled in Fig. 3 correspond to the NN pairs of the Si(001) surface as in Fig. 1b. Among the NN pairs shown in Fig. 1b, the bulk pair b1 is intensely imaged in Fig. 3 as expected already. Among other weak images, two dimer back-bond pairs of d1 and d2 are well reconstructed near the expected positions. The dimer is known to be asymmetric on the Si(001)-(2 × 1) surface and the images d1 and d2 seem to correspond more to the pairs involving upper dimer atoms [12]. A further study is needed to clearly resolve the buckling of dimers.

Then, two questions arise: First, why are only NN pairs strongly imaged in the $P(\mathbf{R})$? Second, why are only the three NN pairs observed in Fig. 3? The answer to the first question is naturally that the vibrational correlation between NN atoms is strong and that the correlation decreases sharply with the increase in interatomic distance. In order to answer the second question, we measured several CTDS patterns with different incidence angles and calculated $P(\mathbf{R})$'s and found that the essential factor is the scattering vector $\mathbf{s}$. Based on the definition, the scattering vector $\mathbf{s}$ forms a narrow cone directing toward x axis, 40° off the surface normal. When we compare the $\mathbf{s}$ direction with the NN bond directions in Fig. 1b, we find that the three NN pairs reconstructed in Fig. 3 have bonds that are nearly parallel to the direction $\mathbf{s}$. We find the same relationship in other $P(\mathbf{R})$'s tested so far.

There are two reasons for the observed $\mathbf{s}$ dependence. First one relies on the background subtraction procedure shown in Eq. (1) [4]. Using the procedure, the oscillation along $\mathbf{s}$ is effectively picked up in χ. However, if the pattern is not oscillating along $\mathbf{s}$ but oscillating along other directions, the whole oscillation might be filtered out by the background subtraction procedure. This condition is realized when the NN bond direction is perpendicular to $\mathbf{s}$. Thus, the NN pairs whose bond direction is nearly perpendicular to $\mathbf{s}$ are removed by the background subtraction. The second reason is the difference in the degree of correlation between the directions parallel and perpendicular to the bond. Generally, the NN vibrational correlation is expected to be stronger along the bond than the direction perpendicular to the bond. Since the scattering coherency is enhanced when MSRD projected on $\mathbf{s}$ is reduced, the NN pair is enhanced in $P(\mathbf{R})$ when the bond direction is parallel to $\mathbf{s}$.

Based on the Debye model, Beni and Platzman [13] predicted that the MSRD of NN atoms of bcc and fcc crystals was 40% reduced at the high temperature limit by the correlation. It is also expected from the Debye model that the correlation quickly drops for the second and third NN's, followed by a further slow decrease with distance [14]. The slow dropping correlation forms the well-known TDS intensity around Bragg spots, and the strong NN correlation forms the present CTDS oscillation. The present method of CTDS will be suitable to probe

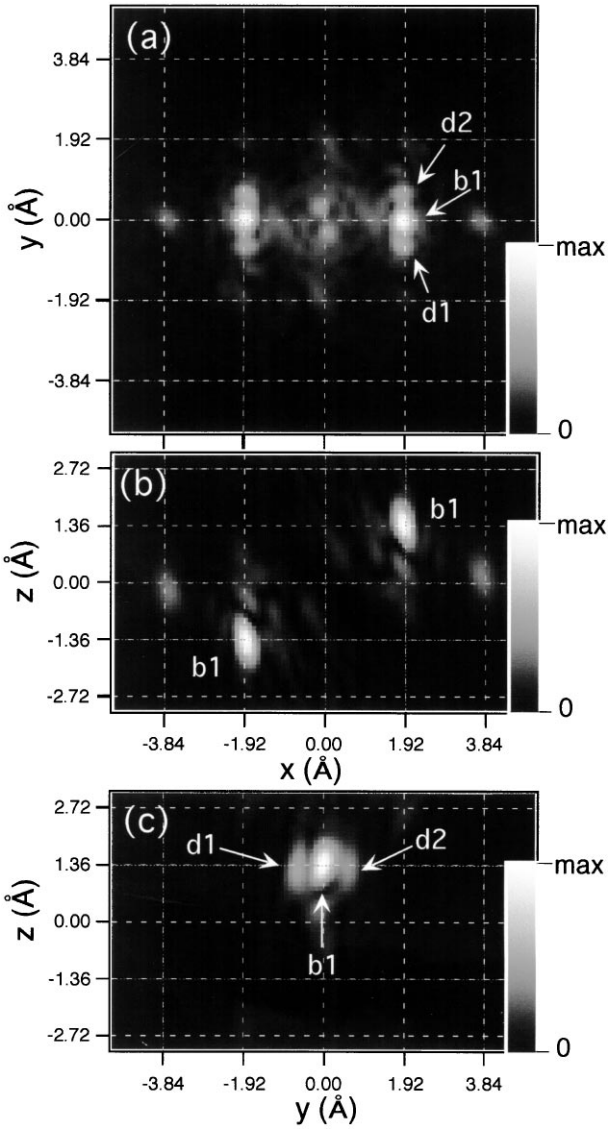

FIG. 3. Patterson function obtained from the experimental χ function in Fig. 2. (a) A projection onto the xy plane. (b) and (c): Cross sections at $y = 0$ and $x = 1.92$ Å, respectively. The dashed lines correspond to the one-layer separation of the Si(001) surface.

the vibrational correlation in more detail if a quantitative formulation can be achieved.

Here, we compare the CTDS of low to medium energy electron diffraction with other holographic methods of structural analysis. As described earlier, CTDS is principally different from EEH's such as DLEED and LEED holography. CTDS is more similar to x-ray diffraction (XRD) than EEH. Compared with XRD, electron diffraction involves the large anisotropic atomic scattering factors and strong MS effect. However, the anisotropy in the scattering factor is manageable in the CTDS by adjusting the incident and emission directions of electrons and can be removed by the background subtraction procedure shown in Eq. (1) [4]. As mentioned earlier, the difficulty of MS effect was overcome by multienergy techniques used in EEH [2–4]. The CTDS is very suited to a multienergy technique since the energy is easily changed. Furthermore, the vibrational correlation is more prominent within a small cluster of atoms, so that there would be less MS paths than in EEH. Therefore, the two main obstacles, i.e., the atomic scattering factor and MS effect, are not serious in CTDS. A high surface sensitivity attained by the grazing incidence is another advantage of CTDS over EEH and XRD as it is demonstrated by the present observation of the dimer back-bond pairs. It is noted that the similar CTDS must be observed in other diffraction techniques, such as XRD, RHEED, and TED, because the present CTDS originates from the crystal vibration itself.

In conclusion, a new structural method of correlated thermal diffuse scattering is presented in which vibrational correlation among the nearest-neighbor atoms plays a key role in low to medium energy electron diffraction. The characteristic of CTDS is to measure 3D intensity distribution of scattered electrons that include up to phonon losses. This is demonstrated for a Si(001) crystal. A 3D CTDS pattern measured for the Si(001)-(2×1) surface with a grazing-incidence electron beam showed a very simple oscillatory pattern that is basically due to interference of electron waves scattered by a NN pair. Patterson function analysis of the 3D CTDS pattern reveals a bulk NN pair and surface dimer back-bond pairs. Quantitative analyses of vibrational correlation of atoms as well as structural studies of solids and solid surfaces will be possible using CTDS.

This work is partly supported by the Grants-in-Aid for Scientific Research (A) (2) (07554051) and Creative Basic Research (09NP1201) of the Ministry of Education, Science, Sports and Culture of Japan.

[1] J. J. Barton, Phys. Rev. Lett. **61**, 1356 (1988).
[2] J. J. Barton, Phys. Rev. Lett. **67**, 3106 (1991).
[3] S. Y. Tong, H. Huang, and C. M. Wei, Phys. Rev. B **46**, 2452 (1992), and references therein.
[4] C. M. Wei, I. H. Hong, and Y. C. Chou, Surf. Rev. Lett. **1**, 335 (1994).
[5] G. R. Harp, D. K. Saldin, and B. P. Tonner, Phys. Rev. Lett. **65**, 1012 (1990).
[6] D. K. Saldin and P. L. de Andres, Phys. Rev. Lett. **64**, 1270 (1990).
[7] C. M. Wei *et al.*, Phys. Rev. Lett. **72**, 2434 (1994); K. Heinz and H. Wedler, Surf. Rev. Lett. **1**, 319 (1994).
[8] K. Reuter *et al.*, Phys. Rev. Lett. **79**, 4818 (1997); K. Reuter *et al.*, Phys. Rev. B **58**, 4102 (1998).
[9] For example, L. V. Azaroff, *Elements of X-ray Crystallography* (McGraw-Hill, New York, 1968).
[10] T. Abukawa *et al.*, J. Electron Spectrosc. Relat. Phenom. **88–91**, 533 (1998).
[11] D. L. Adams and U. Landman, Phys. Rev. B **15**, 3775 (1977).
[12] R. Gunnella *et al.*, Phys. Rev. B **57**, 14 739 (1998).
[13] G. Beni and P. M. Platzman, Phys. Rev. B **14**, 1514 (1976).
[14] J. B. Pendry, in *Low Energy Electron Diffraction* (Academic Press, London, 1974), Chap. 6.